Computational Studies on the Isomeric Structures in the Pyrophosphito Bridged Diplatinum(II) Complex, Platinum Pop†

Gregory I. Gellene* and D. Max Roundhill

Department of Chemistry and Biochemistry, Texas Tech University, Lubbock, Texas 79409-1061

Received: December 31, 2001

Density functional calculations at the B3LYP/LanL2DZ+(f,d,p) level have identified two hydrogen bonding motifs for the title molecule, a C_{4h} eclipsed and a D_4 staggered structure. The eclipsed structure is calculated to be only about 0.8 kcal/mol more stable than the staggered structure when unscaled zero point energies are considered. The two structures can be distinguished in an X-ray crystallographic analysis on the basis of the Pt−P−O−P dihedral angle without the need to explicitly locate hydrogen atoms in the structure. Calculated vibrational frequencies and assignments are generally in very good agreement with the available experimental information. One notable exception to this agreement is the experimentally observed 232 cm^{-1} Raman transition that was previously assigned to a nonspecific ring bending mode and is currently reassigned to the symmetric Pt_2P_8 stretching mode.

Introduction

Square-planar platinum complexes have long been known to exhibit metal−metal interactions in the solid state.[1] These intermetallic interactions can be sufficiently strong that even ions of the same charge can associate in solution media of high dielectric constant. Although unbridged oligomeric metal complexes are not found exclusively in platinum chemistry, they do occur mainly for square-planar metal ions because the vacant axial coordination sites allow the metal centers to approach each other closely. Assuming that the ligands lie in the *xy* plane, the relative *d*-orbital energies are d_{xy}, (d_{xz}, d_{yz}) < $d_z^2 \ll d_{x^2-y^2}$ in d^8 monomer containing π acceptor ligands.[2] This approach along the axial direction causes the valence d_z^2 atomic orbitals to overlap to give bonding ($d\sigma$) and antibonding ($d\sigma^*$) molecular orbitals. Such an orbital energy level diagram has been used to explain the excited-state properties of d^8-d^8 metal−metal dimers.[3,4]

One of the most widely studied d^8-d^8 dimers is the diplatinium(II) complex $Pt_2(\mu\text{-}P_2O_5H_2)_4^{4-}$ (abbreviated Pt_2). This complex contains four bridging (P, P-bonded) pyrophosphito ligands arranged in a face-to-face eclipsed planar structure (Figure 1).[5,6] The excited-state chemistry exhibited by Pt_2 is probably the richest of all d^8-d^8 complexes. Photophysical studies confirm that the properties of the photoactive excited state are a manifestation of d^8-d^8 metal−metal interactions. Much attention has been devoted to the photochemistry of Pt_2 because the observed reactions with substrates include rare examples of atom abstractions, in addition to electron transfers and other well-studied inorganic excited-state processes.[7−9] In addition to the structural and photophysical data on Pt_2, a vibrational analysis has been carried out.[10] This study has identified the Pt−Pt stretching at 116 cm^{-1}, but did not assign any symmetric Pt−P stretching modes in the Raman spectrum.

Although this Pt_2 complex has attracted much attention from photochemists and photophysicists, except for an early extended Hückel calculation,[11] no computational study has been carried out for this complex. This lack of any high level computational information has limited the understanding of the ground-state properties of this complex anion. A consequence of the intramolecular hydrogen bonding between the P−OH and P═O groups is that several isomeric hydrogen bonding motifs are possible. In this study, computational results directed toward obtaining a better understanding of both the structural and vibrational properties of the Pt_2 anion are reported. These results provide insight into how the different hydrogen bonded structures influence the energetics of Pt_2, and suggest an assignment for the symmetric Pt−P stretching mode.

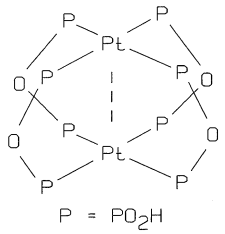

Figure 1. Schematic representation of $Pt_2(\mu\text{-}P_2O_5H_2)_4^{4-}$. Only the P−O−P bridges are shown for clarity.

Methods

All calculations were performed using density functional theory with the hybrid B3LYP method[12] as implemented in the Gaussian 98 (G98) suite of programs.[13] Three basis sets were employed. Preliminary geometry optimizations were performed using the LanLDZ[14,15] basis set which is a full double-ζ (DZ) set for hydrogen and oxygen and an effective core potential (ECP) plus DZ for phosphorus and platinum. The valence electrons are taken to be the 3s and 3p electrons for phosphorus and the 5s, 5p, 5d, and 6s electrons for platinum. The second basis set which was used for the final geometry optimization and harmonic frequency calculations consisted of the LanLDZ set augmented by p polarization functions on hydrogen (ζ = 1.0), d polarization functions on oxygen (ζ = 0.85) and phosphorus (ζ = 0.37), f polarization functions on platinum (ζ = 0.65779643), diffuse sp functions on oxygen (ζ = 0.0845)

† Part of the special issue "G. Wilse Robinson Festschrift".

10.1021/jp0147325 CCC: $22.00
Published on Web 05/01/2002

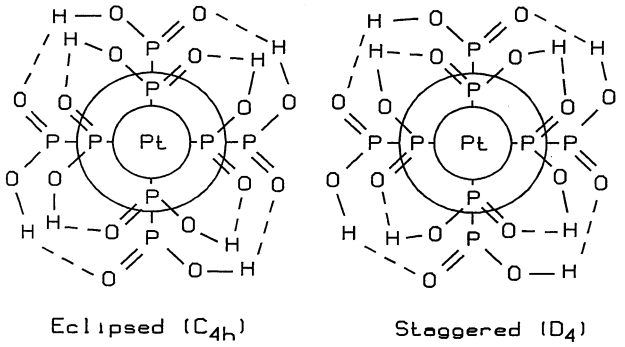

Figure 2. Schematic representations of the C_{4h} eclipsed and the D_4 staggered hydrogen bonding structures of $Pt_2(\mu\text{-}P_2O_5H_2)_4^{4-}$. The view is down the Pt−Pt bond axis with the larger circle representing the eclipsed Pt.

and phosphorus ($\zeta = 0.0348$), and diffuse sp ($\zeta = 0.0147$), and d ($\zeta = 0.0359$) functions on platinum. The ζ (zeta) values for the functions on hydrogen, oxygen, and phosphorus are those recommended for use with the DZ basis set. For platinum, the ζ values for the diffuse functions were optimized following a procedure used for other sixth row atoms[16] and the polarization function was taken from Ahlrichs Coulomb fitting basis set.[17,18] This basis set will be denoted LanLDZ+(f,d,p). The final basis set, which was used for model calculations on $[Pt(POP)_4]^{2-}$, consisted of the LanLDZ basis set for Pt and the all electron, aug-cc-pVDZ basis set[19] for hydrogen, oxygen, and phosphorus. Spherical harmonic angular functions were used throughout. Analytical first derivatives were used to optimize geometries to a residual rms gradient less than 10^{-5} hartree/bohr and analytical second derivatives were used to characterize the stationary points as a local minimum (all real frequencies) or a (hyper)transition state (1 (or more) imaginary frequencies).

Results

Two local minimum energy geometries, which differed principally in the relative orientation of the P−OH···O═P hydrogen bonds around each platinum, were found at the B3LYP/LanLDZ level of calculation. These structures, an eclipsed C_{4h} and a staggered D_4, are shown schematically in Figure 2. At the higher B3LYP/LanLDZ+(f,d,p) level of calculation, the C_{4h} structure remained a local energy minimum, while the D_4 structure was found to be a transition state between equivalent D_2 structures. In going from the D_4 to the D_2 structure, the principle geometric change occurred in the Pt−P−O−P bridging dihedral angles that changed by about 20° but in opposite directions for adjacent bridges. However, this distortion was associated with only a 0.38 kcal/mol decrease in energy. When harmonic zero point energy contributions are considered, the relative stability of these two structures become almost identical with the D_4 structure being only about 0.02 kcal/mol higher in energy than the D_2 structure. This result suggests that the D_2 structure would have a dynamically averaged D_4 structure and thus this geometry will be emphasized in future considerations of the staggered hydrogen bonded motif. The C_{4h} structure, however, was found to be the global minimum energy structure lying about 1.37 kcal/mol below the energy of the D_4 structure at the B3LYP/LanLDZ+(f,d,p) level of calculation. Inclusion of zero point energy places the adiabatic energy of the staggered D_4 structure only 0.84 kcal/mol above that of the eclipsed C_{4h} structure.

A search for a transition state between the staggered and eclipse hydrogen bonding motifs focused on the highly symmetric eclipsed D_{4h} structure where each hydrogen is located symmetrically in a PO···H···OP linkage. At the B3LYP/LanLDZ+(f,d,p) level of calculation, the energy of the D_{4h} structure was found to be 11.50 kcal/mol above that of the C_{4h} structure. However, the harmonic frequency analysis of the D_{4h} structure revealed it to be a hyper-transition state with 10 imaginary frequencies of symmetry species a_{2g}, a_{1u}, e_g, $2e_u$, b_{2u}, and b_{2g}. The a_{2g} and a_{1u} motions are associated with the strongest surface curvature (force constants are ~0.78 mdyn/Å) and lead to the C_{4h} and D_4 structures, respectively. The e_g, one of the e_u, and the b_{2u} motions are associated with a medium surface curvature (force constants are 0.45−0.24 mdyn/Å) and lead to structures having HO−P−OH and O═P═O moieties in various arrangements. The remaining motions (e_u and b_{2g}) are associated with relatively small surface curvature (force constants are 0.025 and 0.001 mdyn/Å, respectively) and lead to structures with nonplanar Pt−P−O−P−Pt rings. Interestingly, the large number of imaginary frequencies for the D_{4h} structure significantly lowers its zero point energy so that the adiabatic energy of the D_{4h} structure is calculated to be 8.07 kcal/mol *below* that of C_{4h} structure. Thus, although it is possible that the C_{4h} and D_4 structures are connected by a transition state having fewer imaginary frequencies, little additional information about the dynamic structure of Pt_2 would be learned by searching for it. This result also suggests that large amplitude distortions of the hydrogen atoms and the associated torsions of the Pt−P−O−P dihedral angles may be feasible motions in Pt_2 even at low temperature. Selected geometric parameters for the C_{4h}, D_4, and D_{4h} structures and the corresponding experimental values[5] are listed in Table 1.

TABLE 1: Comparison of Experimenal[5] and Calculated Geometric Parameters for $Pt_2(\mu\text{-}P_2O_5H_2)_4^{4-}$

parameter	exptl	C_{4h} structure	D_4 structure	D_{4h} structure
		Bond Length/Å		
Pt−Pt	2.925	3.0386	3.0456	2.9658
Pt−P	2.32	2.4035	2.4052	2.3824
P═O	1.52	1.5496	1.5503	1.5892
P−OH	1.68	1.6378	1.6368	1.5892
P−OP	1.62	1.6858	1.6821	1.6856
O−H		1.0223	1.0234	1.2148
		Bond Angle/deg		
P−Pt−P		90.0	90.0	90.0
Pt−P═O		118.1	117.8	113.9
Pt−P−OH		113.1	113.4	113.9
Pt−P−OP		110.0	110.6	111.7
P−O−H		108.9	109.2	109.3
		Dihedral Angle/deg		
Pt−Pt−P═O		113.1	114.6	117.2
Pt−Pt−P−OH		−121.8	−120.4	−117.2
Pt−Pt−P−OP		−11.3	−7.6	0.0
Pt−P−O−P		29.6	4.1	0.0
P−Pt−Pt−P		0.0	7.9	0.0

In C_{4h} symmetry, the 108 normal coordinates of Pt_2 transforms as

$$14a_g \oplus 14b_g \oplus 13e_g \oplus 13a_u \oplus 13b_u \oplus 14e_u \qquad (1)$$

with the a_u and e_u modes (27 modes) being IR active and the a_g and b_g modes (28 modes) being Raman active. Conversely, in D_4 symmetry, the 108 normal coordinates transform as

$$14a_1 \oplus 13a_2 \oplus 13b_1 \oplus 14b_2 \oplus 27e \qquad (2)$$

with the a_2 and e modes (40 modes) being IR active and the a_1, b_1, b_2, and e modes (95 modes) being Raman active. These symmetry considerations significantly reduce the complexity of the possible infrared vibrational spectra. A further reduction in

TABLE 2: Comparison of Experimental[10] and Calculated Transition Energy (cm^{-1}) and Intensity (km/mol) for $Pt_2(\mu\text{-}P_2O_5H_2)_4^{4-}$

	C_{4h} structure		D_4 structure			
exptl energy	energy	intensity (sym)	energy	intensity (sym)	extl assignment	computational assignment
	2800	2783 (e_u)	2784	2855 (e)	NR	OH str
	2739	8 (a_u)	2764	14 (e)		
1329 (IR)	1415	445 (a_u)	1423	324 (a_2)	POH bend	POH bend
	1412	336 (e_u)	1419	448 (e)		
1085 (IR)	1053	1042 (e_u)	1043	905 (e)	P═O str	P═O str
	1021	447 (a_u)	1042	166 (e)		
			1021	462 (a_2)		
910 (IR)	945	123 (e_u)	944	568 (a_2)	P═O str	OH wag
	943	421 (a_u)	941	79 (e)		
			931	22 (e)		
			884	488 (a_2)		
	876	442 (a_u)	804	1 (e)	NR	POP astr
	846	370 (e_u)	839	962 (a_2)	NR	P−OH str
			846	326 (e)		
			848	60 (b_1)		
	834	1080 (a_u)	843	28 (e)	NR	POPastr/P−OH str
695 (IR)	670	344 (e_u)	665	359 (e)	POP str	POPsstr
520 (IR)	529	12 (a_u)	533	11 (a_2)	PO_2 bend	O═P−OH bend
	491	93 (e_u)	499	62 (e)		
			485	23 (e)		
442 (IR)	419	201 (a_u)	419	225 (a_2)	PO_2 bend	O═P−OH wag
360 (IR)	412	12 (e_u)	391	14 (e)	ring bend	PtP−O−PPt wag
			378	5 (a_2)		
335 (IR)	328	13 (a_u)	345	6 (e)	Pt−P str	PtP_4−PtP_4 torsion
308 (IR)	304	39 (e_u)	292	40 (e)	ring bend	O═P−OH rock
278 (IR)	273	6 (e_u)	266	3 (e)	ring bend	P−O−P bend
241 (IR)			256	5 (a_2)		Pt−P═O bend
	257	4 (a_u)	206	2 (e)		P−Pt−P sstr
	246	10 (e_u)				HO_2P−O−PO_2H bend
232 (Raman)	227	(a_g)	239	(a_1)	ring bend	Pt_2P_8 sstr
116 (Raman)	112	(a_g)	107	(a_1)	Pt−Pt str	Pt−Pt str

complexity is achieved by focusing on those modes of a particular type of molecular motion (e.g., OH stretch) that are predicted to have large absorption coefficients. The calculated frequencies of such infrared active modes and their assignment are listed in Table 2 for the C_{4h} eclipsed and the D_4 staggered structures where they are compared with experimental values.[10] Unfortunately, it is not possible to calculate analytical Raman scattering intensities with DFT calculations using ECP basis sets as implemented in G98, so intensity considerations cannot be used to identify the important Raman transitions. However, because only two Raman transitions have been observed for Pt_2, the considerations of Raman active modes in Table 2 is limited to possible assignments for these two transitions.[10]

Discussion

The calculated bond lengths in either the C_{4h} eclipsed, D_4 staggered, or D_{4h} transition state structure is in acceptable agreement with the corresponding experimental[5] bond lengths determined from the X-ray crystallographic study of $K_4[Pt_2(\mu\text{-}P_2O_5H_2]\cdot 2H_2O$. Unfortunately, because no additional molecular structural parameters were reported, the available experimental information is not sufficient to distinguish whether an eclipsed or staggered or both or the D_{4h} dynamically averaged hydrogen bonding motifs were present. Indeed, the detailed nature of the hydrogen bonding pattern was not considered in previous experimental studies. It is worth emphasizing that the present computations indicate that these two local minimum energy structures can be easily distinguished by the Pt−P−O−P dihedral angle allowing these hydrogen bonding motifs to be identified without explicitly locating the hydrogen atoms in the structure. As mentioned previously, this dihedral angle is also a signature parameter for the D_2 staggered structure. Interestingly, the Pt−P bond length variations determined for the crystal structure[5] occur alternately as would be expected for the D_2 staggered structure. However, the magnitude of the experimental variation (0.027 Å) is about 7 times larger than the computational variation (0.004 Å) so that the original explanation[5] of distortions induced by the K^+ ions cannot be discounted. In this same spirit, it should be noted that neither the effects of the counterions and the waters of crystallization in the solid state nor the effects of hydrogen bonding interactions of water in the aqueous state on the relative stability of the C_{4h}, D_4, and D_{4h} structures is known. Further, in aqueous solution, hydrogen bonding interactions with the water solvent may play a role in the conversion between eclipsed and staggered structures. Finally, considering that some aspects of the original crystallographic analysis have been questioned,[6] the detailed nature of the hydrogen bond structure under crystalline and solution conditions must be considered an open question.

The vibrational frequencies for the strong infrared active modes for the C_{4h} eclipsed and the D_4 staggered structures are very similar and generally compare well to the reported transition energies.[10] One notable exception occurs in the region 830−880 cm^{-1} where several strong infrared transitions are predicted for both structures although no transitions in this range were reported. Generally, the computational results fully support the experimental mode assignments with the computational analysis allowing "ring bend" modes to be described in greater detail. However, there are a few experimental assignments that are called into question by the computational results. The band at 910 cm^{-1} is assigned to OH wagging modes rather than the original P═O stretching mode assignment because all the P═O stretching modes are calculated to occur in the range 1020−1055 cm^{-1}. The band at 360 cm^{-1} is assigned to

a PtP_4-PtP_4 torsion mode rather than to a Pt−P stretch as was done originally. A search for Pt−P stretching modes leads to a re-assignment of 232 cm^{-1} transition observed in the Raman specra[10] to the Pt_2P_8 symmetric stretching mode calculated to occur at 227 or 239 cm^{-1} for the C_{4h} and D_4 structures, respectively. The original Pt−P stretching assignment was made on the basis of Pt−P stretching modes[20] occurring at 346 cm^{-1} (IR) and 371 cm^{-1} (Raman) for *trans*-$Pt(PMe_3)_2Cl_2$ and at 347 cm^{-1} (IR) and 370 cm^{-1} (Raman) for *trans*-$Pt(PMe_3)_2I_2$ which were taken as good predictors of the Pt−P stretching modes in Pt_2. To test the present assignment further, B3LYP/aug-cc-pVDZ calculations were performed on $[Pt(PO_3H_2)_4]^{2-}$ (a molecule approximating "half" of Pt_2).[21] Although this basis lacked diffuse and polarization functions on Pt, the result can nevertheless be instructive because the removal of these functions from the LanLDZ+(f,d,p) basis had almost no effect of the relative energy and optimized structures of Pt_2. The $Pt-P_4$ symmetric stretching frequency for $[Pt(PO_3H_2)_4]^{2-}$ was calculated to occur at 258 cm^{-1}, supporting the present reassignment.

Acknowledgment. Acknowledgment is made to the Robert A. Welch Foundation (Grants D-1293 and D-1408) for financial support.

References and Notes

(1) Miller, J. S. *Extended Linear Chain Compounds*; Plenum: New York, 1982; Vols. 1−3.

(2) Cowman, C. D.; Ballhausen, C. J.; Gray, H. B. *J. Am. Chem. Soc.* **1978**, *95*, 7873−7875.

(3) Mann, K. R.; Gordon, J. G., II; Grey, H. B. *J. Am. Chem. Soc.* **1975**, *97*, 3553−3555.

(4) Nocera, D. G.; Maverick, A. W.; Winkler, J. R.; Che, C.-M.; Grey, H. B. *ACS Symp. Ser.* **1983**, *211*, 21−33.

(5) Filomena Dos Remedios Pinto, M. A.; Sadler, P. J.; Neidle, S.; Sanderson, M. R.; Subbiah, A.; Kuroda, R. J. *J. Chem. Soc., Chem. Commun.* **1980**, 13−15.

(6) Marsh, R. E.; Herbstein, F. H. *Acta Crystaollogr., Sect. B* **1983**, *39*, 280−287.

(7) Roundhill, D. M.; Gray, H. B.; Che, C.-M. *Acc. Chem. Res.* **1989**, *22*, 55−61.

(8) Nagle, J. K.; Roundhill, D. M. *Chemtracts: Inorg. Chem.* **1992**, *4*, 141−155.

(9) Kalsbeck, W. A.; Gingell, D. M.; Malinsky, J. E.; Thorp, H. H. *Inorg. Chem.* **1994**, *33*, 3313−3316.

(10) Stein, P.; Dickson, M. K.; Roundhill, D. M. *J. Am. Chem. Soc.* **1983**, *105*, 3489−3494.

(11) Boudreaux, E. A.; Doussa, S. P.; Klobukowski, M. *Int. J. Quantum Chem.: Quantum Chem. Symp.* **1986**, *20*, 239−252.

(12) Stephans, P. J.; Devlin, F. J.; Chabalowski, C. F.; Frisch, M. J. *J. Phys. Chem.* **1994**, *98*, 11623.

(13) Frisch, M. J.; Trucks, G. W.; Schlegel, H. B.; Scuseria, G. E.; Robb, M. A.; Cheeseman, J. R.; Zakrzewski, V. G.; Montgomery, J. A.; Stratmann, R. E.; Burant, J. C.; Dapprich, S.; Millam, J. M.; Daniels, A. D.; Kudin, K. N.; Strain, M. C.; Fakas, O.; Tomasi, J.; Barone, V.; Cossi, M.; Cammi, R.; Mennucci, B.; Pomelli, C.; Adamo, C.; Clifford, S.; Ochterski, J.; Petersson, G. A.; Ayala, P. Y.; Cui, Q.; Morokuma, K.; Malick, D. K.; Rabuck, A. D.; Raghavachari, K.; Forseman, J. B.; Cioslowski, J.; Ortiz, J. V.; Stefanov, B. B.; Liu, G.; Liashenko, A.; Piskorz, P.; Komaroni, I.; Gomperts, R.; Martin, R. L.; Fox, D. J.; Keith, T.; Al-Laham, M. A.; Peng, C. Y.; Nanayakkara, A.; Gonzalez, C.; Challacombe, M.; Gill, P. M. W.; Johnson, B. G.; Chen, W.; Wong, M. W.; Andres, J. L.; Head-Gordon, M.; Repologle, E. S.; Pople, J. A. *Gaussian 98*, Revision A.6; Gaussian, Inc.: Pittsburgh, PA, 1998.

(14) Wadt, W. R.; Hay, P. J. *J. Chem. Phys.* **1985**, *82*, 284−298.

(15) Wadt, W. R.; Hay, P. J. *J. Chem. Phys.* **1985**, 299−310.

(16) Check, C. E.; Faust, T. O.; Baily, J. M.; Wright, B. J.; Gilbert, T. M.; Sunderlin, L. S. *J. Phys. Chem. A*, **2001**, *105*, 8111.

(17) Eichkorn, K.; Treutler, O.; Ohm, H.; Haser, M.; Ahlrichs, R. *Chem. Phys. Lett.* **1995**, *240*, 283−290.

(18) Eichkorn, K.; Weigend, F.; Treutler, O.; Ahlrichs, R. *Theor. Chem. Acc.* **1997**, *97*, 119−124.

(19) Woon, D. E.; Dunning, T. H., Jr. *J. Chem. Phys.* **1993**, *98*, 1358.

(20) Duddell, D. A.; Goggin, P. L.; Goodfellow, R. J.; Norton, M. G.; Smith, J. G. *J. Chem. Soc. A.* **1970**, 545−564.

(21) Troitskaya, A. D. *Russ. J. Inorg. Chem.* **1961**, *6*, 585.